Endoplasmic reticulum stress induces renal fibrosis in high-fat diet mice via the TGF-β/SMAD pathway

ZHIDAN MU[1], BIN LI[1], MINGYANG CHEN[1], CHEN LIANG[1], WEI GU[2] and JUAN SU[1]

[1]Department of Physiology and Pathophysiology, College of Basic Medicine, Dali University, Dali, Yunnan 671000, P.R. China;
[2]Department of Infection Disease, First Affiliated Hospital of Dali University, Dali, Yunnan 671000, P.R. China

Abstract. The aim of the present study was to investigate the role and mechanism of endoplasmic reticulum stress (ERS) in kidney injury caused by high-fat diet (HFD). An obese mouse model was established via HFD feeding and intervention was performed by intraperitoneal injection of the ERS inhibitor salubrinal (Sal). Changes in the body and kidney weight and serum biochemical indices of the mice were determined. Hematoxylin and eosin and Masson staining were used to observe the pathological changes of renal tissues. Reverse transcription-quantitative PCR and western blotting were used to observe the expression of ERS-related proteins and TGF-β/SMAD pathway-related proteins. Immunohistochemistry was employed to explore the distribution of these proteins. Compared with those in the control group, the weight gain, lipid metabolism disorders and deterioration of renal function in the model group were greater. Malondialdehyde was elevated and superoxide dismutase was decreased in renal tissues. The mRNA and protein levels of TGF-β1, SMAD2/3, α-smooth muscle actin, collagen I, glucose-regulated protein 78 and C/EBP-homologous protein were markedly elevated, whereas SMAD7 was markedly decreased. Sal markedly inhibited the aforementioned effects. This investigation revealed a link between ERS and renal injury caused by HFD. ERS in HFD-fed mice triggers renal fibrosis through the TGF-β/SMAD pathway.

Introduction

The incidence rate of obesity has been increasing rapidly in the past few years and obesity has become a crucial health issue and the most serious epidemic threatening human health (1). Chronic kidney disease (CKD) and cardiovascular illnesses are both significantly affected by obesity (2). Studies have shown that metabolic syndrome, obesity and being overweight are important separate indicators of risk for CKD and end-stage renal disease (ESRD) (1,3). The dominant pathological characteristic of CKD is renal fibrosis, which is accompanied by sparse blood vessels and morphological manifestations such as tubular atrophy, glomerulosclerosis and chronic interstitial inflammation (4). Although the precise mechanisms underlying the promotion of renal fibrosis by obesity, metabolic problems and inflammatory responses resulting from a high-fat diet (HFD) remain unclear, numerous investigations have supported this finding (5-7).

One of the most vital organelles in the cell, the endoplasmic reticulum (ER), is responsible for a number of vital processes, including protein synthesis, folding, maturation and Ca^{2+} storage. It also greatly affects the movement of materials inside cells (8). Misfolded and unfolded proteins may accumulate as a result of ER malfunction, which can initiate the unfolded protein response (UPR) and endoplasmic reticulum stress (ERS) (9). ERS is an important self-defense mechanism of the body that aims to maintain the stability of the ER environment to ensure its normal physiological functions (10). However, excessive UPR activity can harm the ER and cause impaired protein function or cell death through the accumulation of a number of misfolded proteins in the ER (11).

A crucial aspect of the lipid metabolism problem is ERS. Numerous investigations conducted in the last few years have demonstrated a strong correlation between ERS and the development of hyperlipidemic complications (12-14). However, whether ERS plays a role in kidney damage caused by HFD and its exact molecular mechanisms are unclear. The present study verified that ERS promoted renal fibrosis in HFD-fed mice and revealed that ERS may play an important role in regulating the TGF-β/SMAD signaling pathway.

Materials and methods

Animals. A total of 30 3-week-old C57BL/6J male mice (certificate no: SCXK 2019-0010) weighing 10-12 g were obtained from SPF (Beijing) Biotechnology Co. Animal institutions housed mice free of viruses and parasites. A 12-h light/dark cycle with an ambient environment of 24-26°C and

Correspondence to: Professor Juan Su, Department of Physiology and Pathophysiology, College of Basic Medicine, Dali University, 22 Wanhua Road, Dali, Yunnan 671000, P.R. China
E-mail: 616sj@163.com

Professor Wei Gu, Department of Infection Disease, First Affiliated Hospital of Dali University, 22 Wanhua Road, Dali, Yunnan 671000, P.R. China
E-mail: gw777@163.com

a humidity level of 50-65% was used for the mice. Before the experiment, all the mice were acclimated and fed for one week. A total of 10 mice per group were assigned randomly to the control, the HFD and the HFD + Sal groups. The National Experimental Animal Feeding Guidelines were followed and the Dali University Animal Ethics Committee approved all animal uses (approval no. 2023-PZ-278).

Establishment of the animal model and specimen harvesting. Control mice were fed a regular chow diet and HFD mice were fed a high-fat diet with a fat-to-energy ratio of 60%. The mice in the HFD group weighed 20% more than those in the control group, indicating successful modeling (15). The HFD + Sal group received a daily intraperitoneal injection of 1 mg/kg of salubrinal solution (16). The mice were observed at a fixed time every day for diet, water intake, body posture, behavior and response to external stimuli. The body weights of the mice were measured each week. Animals were humanely euthanized if they reached the humane endpoint [>15% weight loss or >20% overall weight loss within 1-2 days or showing obvious signs of distress (lethargy, squinting, dehydration, hunching)]. However, no such cases were observed in the present experiment. The mice were all kept under standard conditions for 10 weeks and then harvested. The mice were passively fasted for 12-14 h before surgery without access to drinking water. Mice were anesthetized by intraperitoneal injection of sodium pentobarbital solution 50 mg/kg and 0.5-1 ml blood was collected by cardiac puncture and sacrificed by cervical dislocation. The blood was centrifuged at 4°C for 10 min at 1,000 x g. The serum was separated and subjected to biochemical analysis. After blood collection, the kidneys were removed, rinsed and rapidly weighed. The left kidney of mice were submerged in liquid nitrogen at -80°C for later experiments. The right kidney was then preserved in a 4% paraformaldehyde solution at room temperature for 24 h for histological analysis.

Blood biochemistry analysis. The serum-related indicators of the mice were detected via test kits for total cholesterol (TC; cat. no. A111-1-1), triglyceride (TG; cat. no. A110-1-1), low-density lipoprotein (LDL; cat. no. A113-1-1) and high-density lipoprotein (HDL; cat. no. A112-1-1) to assess whether the obese model was successfully established. The renal function of the mice was assessed using a test kit for creatinine (Cr; cat. no. C011-2-1), blood urea nitrogen (BUN; cat. no. C013-2-1) and uric acid (UA; cat. no. C012-2-1). Superoxide dismutase (SOD; cat. no. A001-3) and malondialdehyde (MDA; cat. no. A003-2) were detected to analyze oxidative stress. The kits used were from Nanjing Jiancheng Bioengineering Institute.

Hematoxylin and eosin (H&E) staining. After being cleaned with regular saline, the kidney tissue was preserved with 4% paraformaldehyde at room temperature and subjected to gradient dehydration in ethanol. The tissue blocks were placed in molds containing wax solution and left to cool and solidify on a freezer table for 10 min before removal. The embedded tissue was continuously sectioned with a microtome at a thickness of 4-5 μm. The sections were stained using hematoxylin for 8 min and eosin for 5 min at room temperature. The renal morphology of each group was examined microscopically.

A total of three kidneys were selected from each group and 10 non-overlapping regions were randomly selected from each kidney at x40 magnification.

Masson staining. The Masson three-color staining procedure was used to assess the severity of renal fibrosis. Kidney samples were extracted as soon as possible after death and stored in 4% paraformaldehyde at room temperature. After rinsing the kidney tissues with PBS, complete dehydration was performed at 50, 70, 80, 95 and 100% starting with 30% ethanol. The tissue blocks were placed in molds filled with wax solution, cooled and solidified on a freezer table for 10 min, and then removed for sectioning. At room temperature, sections were stained with hematoxylin staining solution for 5 min, Ponceau acid fuchsin staining solution for 10 min, and finally stained with bright green staining solution for 1 min. The degree of collagen accumulation in renal interstitial fibrosis was observed via Masson's trichrome staining. The blue linear or granular deposits were positive for collagen. Sections were observed under light microscopy and analyzed semi-quantitatively using ImageJ v1.8.0 software (National Institutes of Health).

Immunohistochemistry. Paraffin sections of 4 μm renal tissue were deparaffinized with xylene at 50°C for 3 min, hydrated by graded ethanol series and then incubated in 3% hydrogen peroxide at room temperature for 15 min to inactivate endogenous peroxidase. After washing with PBS, sections were blocked with 5% goat serum (Beyotime Institute of Biotechnology) for 60 min. Sections were incubated overnight at 4°C with primary antibodies as follows: Grp78 (Proteintech Group, Inc.; cat. no. 11587-1-AP; 1:200), CHOP (Wuhan Servicebio Technology Co., Ltd.; cat. no. GB11204; 1:500), α-SMA (Cell Signaling Technology, Inc.; cat. no. 19245; 1:400), collagen I (Chengdu Zen-Bioscience Co., Ltd.; cat. no. 343277; 1:100), TGF-β1 (Wuhan Boster Biological Technology, Ltd.; cat. no. BA0290; 1:100), Phospho-SMAD2/3 (Affinity Biosciences; cat. no. AF3367; 1:100) and SMAD7 rabbit pAb (ABclonal Biotech Co., Ltd.; cat. no. A12343; 1:100). Sections were incubated with secondary antibody (Wuhan Servicebio Technology Co., Ltd.; cat. no. G1214; 1:200) for 1 h at room temperature and stained with 3,3'-diaminobenzidine (DAB) for 5 min at room temperature and counterstained with hematoxylin for 60 sec at room temperature. Sections were observed under a light microscope at 40x magnification and analyzed semi-quantitatively using ImageJ v1.8.0 software (National Institutes of Health).

Reverse transcription-quantitative (RT-q) PCR. Total RNA was isolated from kidney Tissue (20 mg) using the Fast pure® Cell/Tissue Total RNA Isolation Kit (Vazyme, China). Then, the RNA was reverse transcribed into cDNA using the HiScript®III RT SuperMix for qPCR kit (Vazyme). The qPCR reaction system was then prepared using 2xChamQ Universal SYBR qPCR Master Mix (Vazyme, China). RNA extraction, cDNA synthesis and qPCR were performed according to the manufacturer's protocol. The Step One Real-time PCR apparatus (StepOnePlus; Applied Biosystems; Thermo Fisher Scientific, Inc.) was subsequently used to conduct RT-qPCR. Thermocycling conditions were as follows: 95°C for 30 sec, followed by 40 cycles at 95°C for 30 sec and 60°C for 30 sec. Finally, the reaction was completed

Table I. PCR primer nucleotide sequences used during the research.

Gene	Forward primer	Reverse primer
CHOP	CCAGGAAACGAAGAGGAAGAAT	CACTGACCACTCTGTTTCCGTTT
GRP78	CGCACTTGGAATGACCCTT	CATCTTTGGTTGCTTGTCGC
α-SMA	TCAGGGAGTAATGGTTGGAATG	CCAGAGTCCAGCACAATACCAG
Collagen I	GGTCCTGCTGGTCCTGCTG	GAGAAGCCACGATGACCCTTTATG
TGF-β1	GCTGAACCAAGGAGACGGAATA	GGCTGATCCCGTTGATTTCC
Smad2	TCGTCCATCTTGCCATTCACTCC	CCATTCTGCTCTCCACCACCTG
Smad3	AGCCCCAGAGCAATATTCCAG	GACATCGGATTCGGGGAGAG
Smad7	AGCCGCCCTCGTCCTACTC	GATTCACAGCAACACAGCCTCTTG
GAPDH	GGCAAATTCAACGGCACAGTCAAG	TCGCTCCTGGAAGATGGTGATGG

at 95˚C for 15 sec, 60˚C for 60 sec, and 95˚C for 15 sec. The reaction volume was 10 μl. The relative expression of each gene was determined by the $2^{-\Delta\Delta Cq}$ method (17). These experiments were repeated three times. Table I details PCR primers for C/EBP-homologous protein (CHOP), glucose-regulated protein 78 (GRP78), α-smooth muscle actin (α-SMA), Collagen I, TGF-βl, SMAD2, SMAD3 and SMAD7.

Western blot analyses. Western blotting was used to assess the expression of ERS-associated proteins (GRP78 and CHOP), α-SMA, collagen I and pathway-associated proteins. Renal tissues from the mice in each experimental group were placed in precooled RIPA lysis buffer (Beyotime Institute of Biotechnology), homogenized with an electric homogenizer and then centrifuged at 4˚C. The BCA quantitative measurement method was used to assess the protein concentration of the supernatant. Sample buffer and RIPA buffer were used to prepare the samples to ensure that the amounts of the three sets of protein samples were equal. The loading volume of each group was 5 μl and the proteins were separated via 10% SDS-PAGE. A Bio-Rad rotary membrane device (Bio-Rad Laboratories, Inc.) was then used to transfer the proteins from the gel onto the PVDF membrane. The PVDF membranes were incubated with primary antibodies overnight at 4˚C after being blocked for 30 min at ambient temperature via a quick blocking solution (Shanghai share-bio Biotechnology Co., Ltd.). The antibody dilutions used were as follows: β Actin monoclonal antibody (Proteintech Group, Inc.; cat. no. 66009-1-lg; 1:6,000), GRP78 rabbit polyclonal antibody (Proteintech Group, Inc.; cat. no. 11587-1-AP; 1:3,000), CHOP/GADD153 monoclonal antibody (Proteintech Group, Inc.; cat. no. 66741-1-lg; 1:3,000), anti-TGF-β1 (Wuhan Boster Biological Technology, Ltd.; cat. no. BA0290; 1:1,000), SMAD2/3 rabbit mAb (Cell Signaling Technology, Inc.; cat. no.8685; 1:1,000), phosphorylated (p-)SMAD2/SMAD3 rabbit mAb (Cell Signaling Technology, Inc.; cat. no.8828; 1:1,000), SMAD7 rabbit pAb (ABclonal Biotech Co., Ltd.; cat. no. A12343; 1:1,000), α-SMA (Cell Signaling Technology, Inc.; cat. no.19245; 1:1,000) and collagen I (Chengdu Zen-Bioscience Co., Ltd.; cat. no. 343277; 1:1,000). The membranes were incubated with secondary antibodies (Proteintech Group, Inc.; cat. no. SA00001-2; 1:6,000) for 90 min the following day. The images were developed with a sensitive ECL chemiluminescence kit, exposed and scanned with a chemiluminescence

imager. For proteins with the same molecular weight as the internal reference, an antibody was applied to the target protein first, then developed with a luminescent kit and then eluted with an antibody eluent (which removes the antibody bound to the membrane without affecting the antigen protein). Upon completion, the membrane was developed again to ensure that it has been thoroughly eluted, then the developer was washed with TBST (0.1% Tween-20) and finally the β-actin antibody was applied and developed again. ImageJ v1.8.0 software (National Institutes of Health) was used for semiquantitative analysis, with β-actin used as an internal reference.

Statistical analysis. The expression values for all the experimental data were presented as the means ± standard deviation (n=5). One-way analysis of variance (ANOVA) was used to compare three or more groups with Tukey's post hoc test. For comparisons, unpaired t-test was used to compare two groups. Statistics were analyzed with GraphPad Prism 9.0 software (Dotmatics). P<0.05 was considered to indicate a statistically significant difference.

Results

Change in weight and blood lipid levels in mice. To determine whether the obesity model had been successfully established, the following indicators were first examined. Compared with those in the control group, the body weights of the model group mice increased significantly (P<0.0001), whereas following Sal intervention, the body weights of the model group mice decreased (P<0.01; Fig. 1A). Compared with those in the control group, the blood levels of TG, TC and LDL in the model group were significantly greater (P<0.01), whereas the HDL level in the model group was lower (P<0.05). Compared with the model group, serum levels of TG, TC and LDL in HFD + Sal group were decreased (P<0.05), while HDL levels were increased (P<0.05; Fig. 1B-E). These findings demonstrated that the present study successfully established a mouse obesity model and that the abnormal lipid metabolism induced by HFD in mice could be ameliorated by Sal treatment.

Changes in renal function and morphology in mice. Next, blood biochemical markers were assessed to determine the renal function of the mice and the level of kidney damage was observed
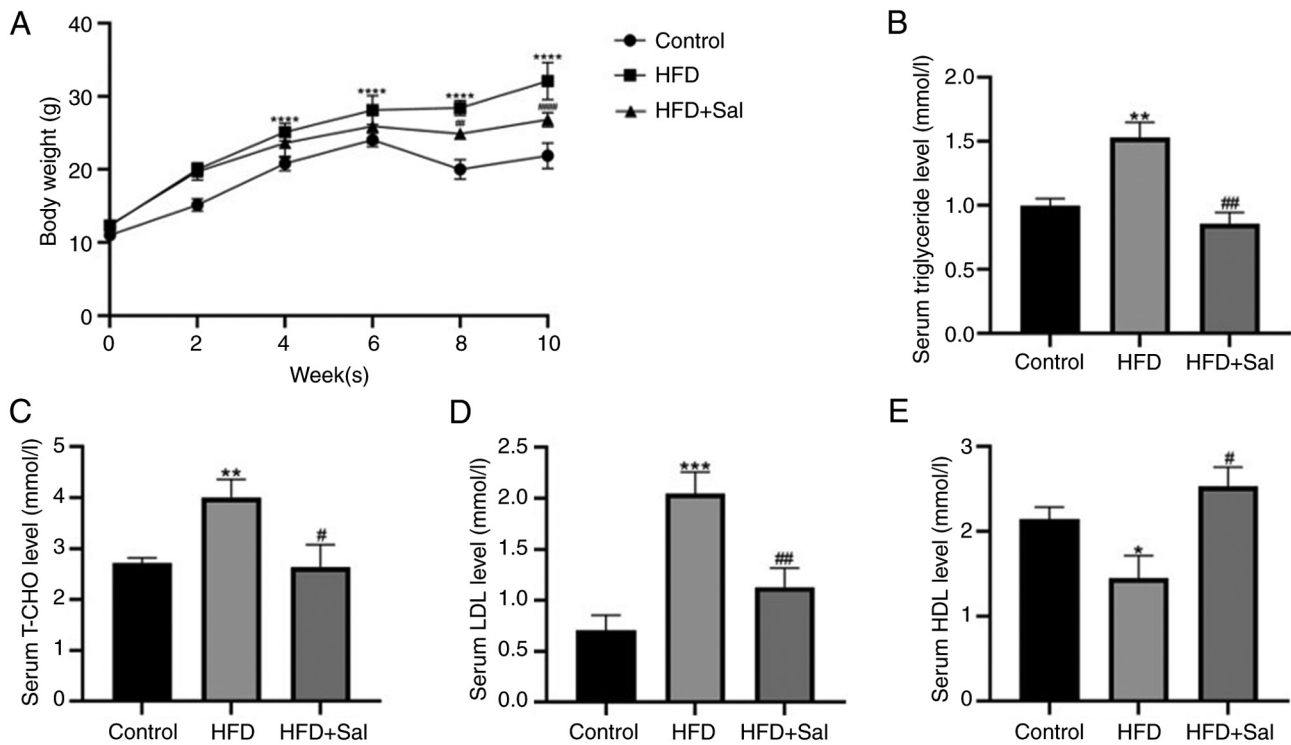
Figure 1. Changes in weight and blood lipid levels in mice. (A) Weight gain curves of the mice. (B) Serum triglyceride, (C) T-CHO, (D) LDL and (E) HDL levels. *$P<0.05$, **$P<0.01$, ***$P<0.001$, ****$P<0.0001$ vs. the control group; #$P<0.05$, ##$P<0.01$, ####$P<0.0001$ vs. the HFD group. T-CHO, LDL and HDL.

via HE staining. As shown in Fig. 2A, the renal body ratio of the model mice was lower than those of the control mice ($P<0.05$) and it increased in the model mice following Sal intervention, but the difference was not statistically significant. Fig. 2B-D shows that the serum levels of Cr, BUN and UA in the model group were greater than those in the control group ($P<0.05$), indicating that renal function was impaired. However, the levels of these markers significantly decreased in the model group after they received Sal ($P<0.05$), indicating that Sal potentially improved renal function in HFD-fed mice. Next, the degree of oxidative stress in the three groups of mice was assessed. The model group had lower levels of the oxidative stress indicator SOD ($P<0.001$) and greater amounts of MDA ($P<0.05$) than did the control group. Sal decreased oxidative stress in HFD-fed mice, as evidenced by the fact that Sal intervention increased SOD ($P<0.01$) and decreased MDA ($P<0.0001$) in the model group (Fig. 2E-F). HE staining revealed that the control group had a regular renal tissue structure. Compared with those in the control group, the glomeruli in the HFD group grew, the mesangium increased and the brush border of the proximal tubules was more severely damaged, indicating vacuolization. Moreover, Sal considerably decreased the aforementioned pathological alterations (Fig. 2G). These findings indicate that HFD exacerbates renal dysfunction and kidney damage in mice, both of which are partially repaired by Sal.

Activation of ERS in mice. To determine ERS activation in mice, the levels of the ERS-related proteins CHOP and GRP78 were examined. RT-qPCR and western blotting were employed to assess gene and protein levels in renal tissues. CHOP and GRP78 gene and protein levels in the model group were significantly higher than those in the control group ($P<0.01$). In the model group, the

CHOP and GRP78 gene and protein levels were decreased by Sal intervention ($P<0.01$; Fig. 3A-E). Immunohistochemistry was used to detect the expression and location of these two proteins. The positive expression of CHOP and GRP78 in the model group was significantly higher than those in the control group ($P<0.05$). Sal partially reversed the HFD-induced increases in GRP78 and CHOP ($P<0.05$; Fig. 2F). According to the aforementioned findings, HFD-fed mice have markedly triggered ERS.

Degree of renal fibrosis in mice. Masson staining revealed the production and deposition of collagen in the renal tissue. As demonstrated by the results of Masson's trichrome staining, the renal tissue of the control group contained normal glomeruli and tubules with minimal blue staining. The model group displayed a substantial amount of collagen fiber stripes in their renal interstitium. These stripes were stained blue, indicating a clear case of renal interstitial fibrosis. Compared with the model group, the Sal group presented a partial reduction in the area of blue-positive staining, as well as a decrease in collagen accumulation in renal tissue and a reduction in renal interstitial fibrosis (Fig. 4A). Furthermore, Fig. 4B and C shows that the renal tissue of the model group expressed higher α-SMA and collagen I gene levels than did the control group ($P<0.05$). Sal significantly decreased the α-SMA and collagen I gene levels that were elevated by HFD ($P<0.01$). As depicted in Fig. 4D-F, the renal tissue levels of the α-SMA and collagen I proteins in the model mice were considerably greater than those in the control mice ($P<0.001$), whereas following Sal treatment, the α-SMA and collagen I protein levels in the HFD-fed mice were significantly lower ($P<0.001$). The expression and localization results of the two proteins shown by immunohistochemistry in Fig. 4G revealed that, compared with those in the control group, α-SMA expression was significantly
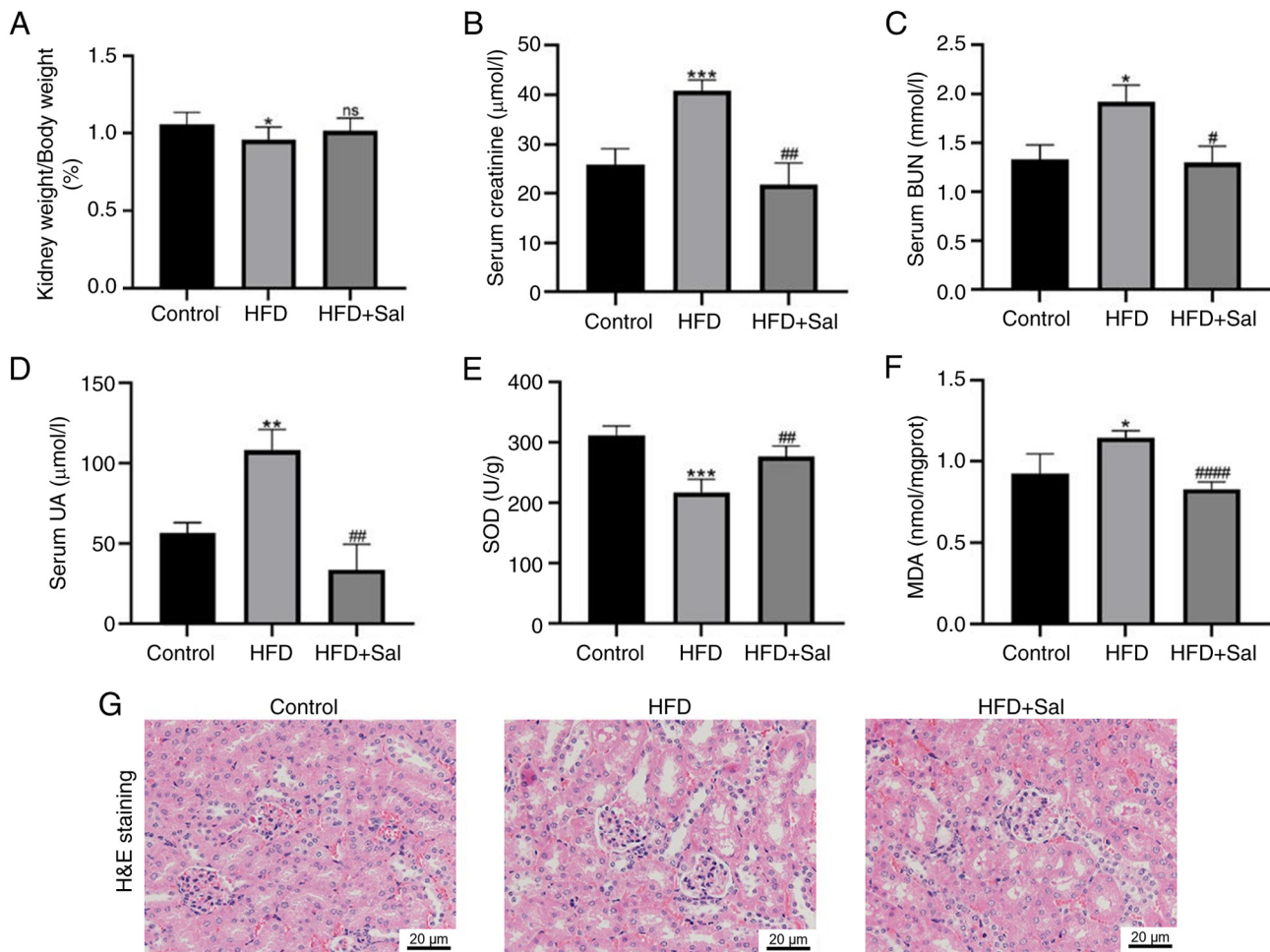
Figure 2. Changes in renal function and morphology in mice. (A) The renal-to-body weight ratio in the mice. (B) Serum creatinine, (C) BUN and (D) UA levels. Kidney (E) SOD and (F) MDA levels. *$P<0.05$, **$P<0.01$, ***$P<0.001$ vs. the control group; #$P<0.05$, ##$P<0.01$, ####$P<0.0001$ vs. the HFD group; ns, not significant. (G) Hematoxylin and eosin staining for pathological changes in renal tissue. Scale bar, 20 μm; magnification, x400. BUN, blood urea nitrogen; UA SOD, superoxide dismutase; MDA, malondialdehyde; HFD, high-fat diet; Sal, salubrinal.

greater in the renal tubulointerstitium and collagen I was significantly expressed at the intersection of the renal cortex and medulla in HFD-fed mice ($P<0.05$). Notably, a substantial decrease in the α-SMA and collagen I levels was detected in the Sal group compared with the model group ($P<0.05$). These findings suggested that HFD-induced ERS exacerbated renal fibrosis in mice and that this is mitigated by Sal.

Activation of the TGF-β/SMAD pathway. Sal was previously shown to ameliorate HFD-induced renal fibrosis in mice. However, it is uncertain what molecular mechanism is responsible for this improvement. Earlier work has indicated that TGF-β/SMAD signaling, particularly SMAD2/3 and SMAD7, is involved in the growth and progression of fibrosis (18). Consequently, the TGF-β/SMAD pathway-associated protein expression levels was examined in the three different groups. Using RT-qPCR, the present study identified the mRNA levels of TGF-β1, SMAD2, SMAD3 and SMAD7. Fig. 5A-D shows that in the renal tissue of the model group, the TGF-β1, SMAD2 and SMAD3 gene levels were greater ($P<0.05$) and the SMAD7 gene level was lower than those in the control group ($P<0.01$). Sal intervention resulted in a decrease in TGF-β1, SMAD2 and SMAD3 gene expression ($P<0.05$)

and an increase in SMAD7 gene expression in renal tissue ($P<0.001$). The protein expression of these genes was determined via western blot analysis. Fig. 5E-H shows higher levels of TGF-β1 and p-SMAD2/3 expression in the model mice compared with the controls ($P<0.0001$), whereas the SMAD7 level was lower ($P<0.0001$). Sal markedly decreased the levels of these two proteins in HFD-fed mice ($P<0.001$) and increased the SMAD7 level ($P<0.0001$). As shown in Fig. 5I, immunohistochemical staining of renal tissues revealed that, compared with the control group, the model group markedly increased the TGF-β1 and p-SMAD2/3 levels ($P<0.0001$) but significantly downregulated the expression of SMAD7 ($P<0.01$). In addition, Sal partly reversed the increases in the TGF-β1 and p-SMAD2/3 levels ($P<0.01$) and the decrease in the SMAD7 level caused by HFD ($P<0.05$). In summary, Sal regulated the TGF-β/SMAD pathway to diminish renal fibrosis in HFD-fed mice and ERS probably involved the same mechanism to worsen renal fibrosis in HFD-fed animals.

Discussion

Obesity has emerged as a prominent independent danger marker for CKD and ESRD in the age of the obesity epidemic (19).
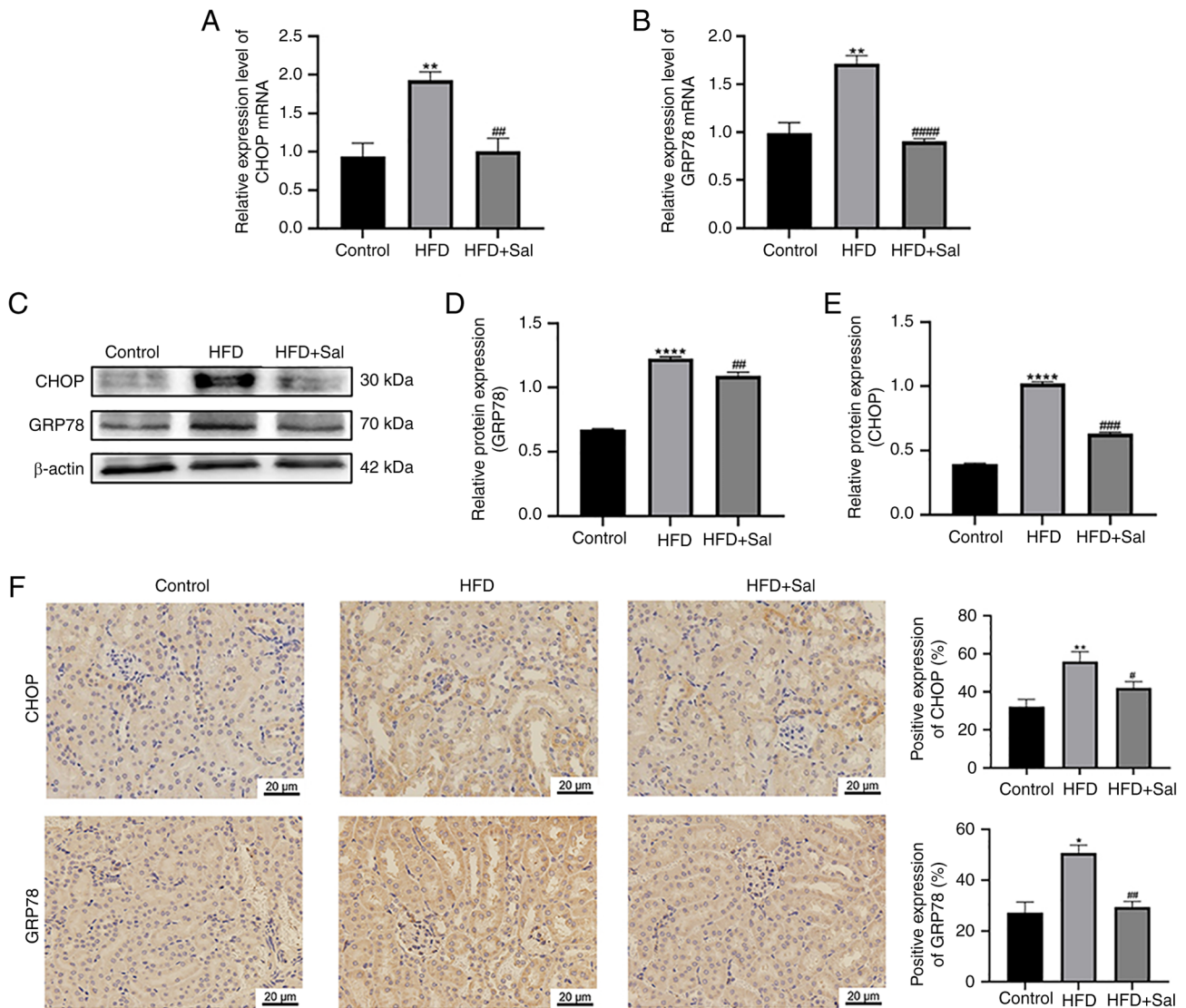
Figure 3. Activation of ERS in mice. The mRNA levels of (A) CHOP and (B) GRP78. (C-E) Western blotting for the levels of proteins, including CHOP and GRP78. **P<0.01, ****P<0.0001 vs. the control group; ##P<0.01, ###P<0.001, ####P<0.0001 vs. the HFD group. (F) Kidney tissues were immunohistochemically stained for CHOP and GRP78. Scale bar, 20 μm; magnification, x400; n=3. *P<0.05, **P<0.01 vs. the control group; #P<0.05, ##P<0.01 vs. the HFD group. ERS, endoplasmic reticulum stress; CHOP, C/EBP-homologous protein; GRP78, glucose-regulated protein 78; HFD, high-fat diet; Sal, salubrinal.

Hsu *et al* (20) report that being overweight or obese is a risk factor associated with CKD in a sizable cohort consisting of adults in northern California; Iseki *et al* (21) arrives at the same conclusion, demonstrating that obesity markedly increases the relative risk of CKD in older individuals. These results suggest that obesity is closely related to CKD. One prevalent pathological characteristic of CKD is renal fibrosis, which is a predictor of progression to ESRD (22). HFD is closely related to renal fibrosis. HFD feeding stimulates lipogenic enzymes in the fatty acid synthesis pathway but inhibits lipolysis, which subsequently drives the excessive accumulation of lipids in the kidney. Altered lipid metabolism ultimately leads to kidney injury, including glomerulosclerosis, interstitial fibrosis and proteinuria (23). One study reveals that mice fed HFD for 12 weeks develop obesity, insulin resistance and oxidative stress, leading to liver and kidney fibrosis (5). The present study confirmed the successful establishment of an obese mouse model in which the mice in the HFD group had significantly greater body weights and elevated serum TG and TC levels

compared with those in the control group, suggesting that the mice in the HFD group had severe fat accumulation and were unable to carry out normal lipid metabolism. Masson's trichrome staining revealed that the mice in the HFD group presented increased deposition of collagen fibers, suggesting that renal fibrosis was severe in this group. Moreover, epithelial-mesenchymal transition (EMT) is an important cause of renal interstitial fibrosis (24). It can lead to the upregulation of fibronectin and fibroblast marker (α-SMA) expression (25). The findings of the present study also confirmed that the expression of α-SMA and collagen I was elevated in the HFD group compared with the control group. In addition, the content of the lipid peroxide MDA was elevated in the renal tissues of the mice in the HFD group, whereas the content of the antioxidant enzyme SOD was decreased, suggesting that excessive lipid accumulation induced oxidative stress and consequently damage to renal tissues. Therefore, it was hypothesized that HFD-fed mice accumulated lipids, leading to disorders of lipid metabolism, which in turn promoted renal
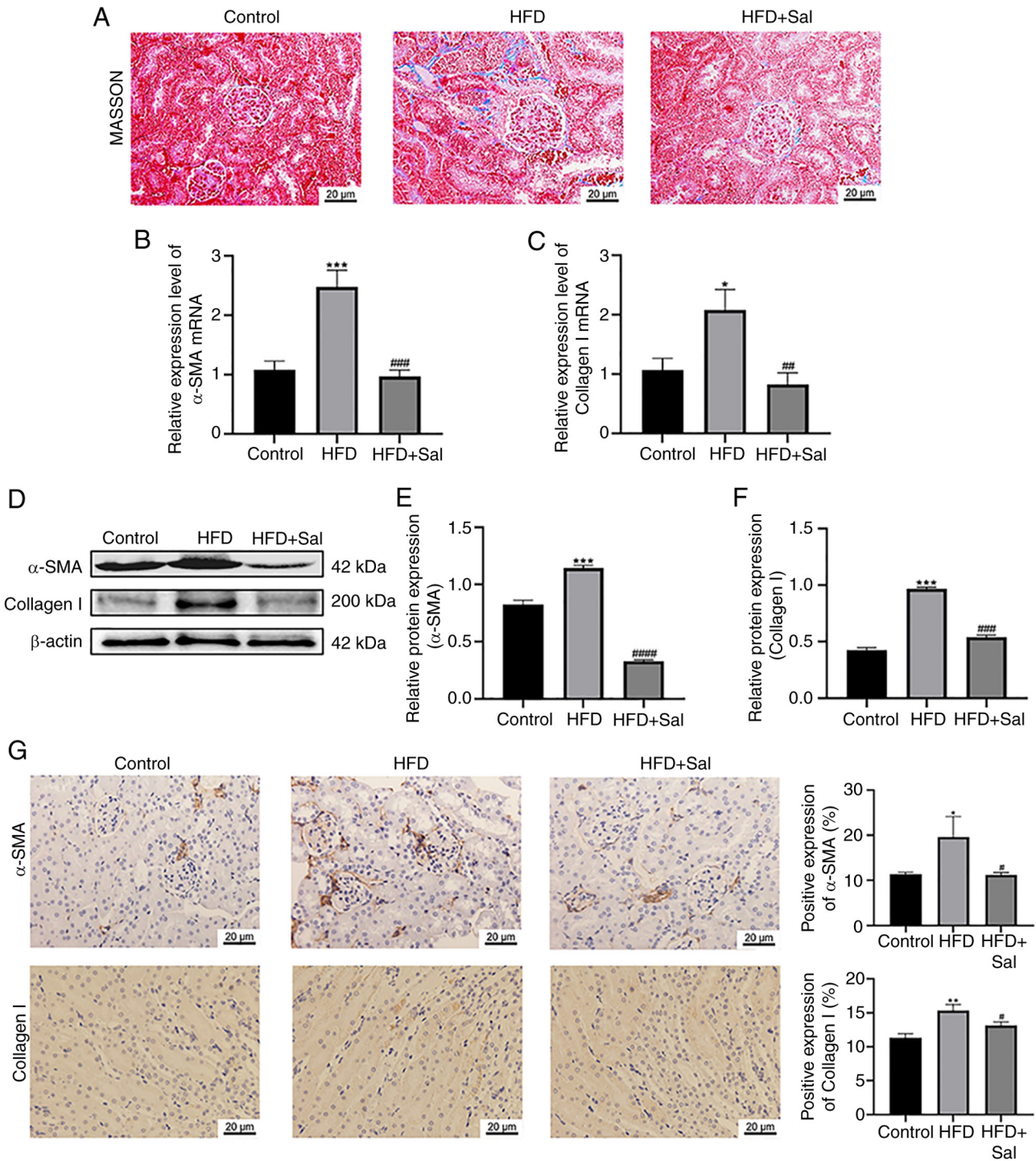
Figure 4. Degree of renal fibrosis in mice. (A) Representative sections from the three groups are shown. Scale bar, 20 μm; magnification, x400. The mRNA levels of (B) α-SMA and (C) collagen I. (D-F) Western blotting for the levels of proteins, including α-SMA and collagen I. $^*P<0.05$, $^{***}P<0.001$ vs. the control group; $^{##}P<0.01$, $^{###}P<0.001$, $^{####}P<0.0001$ vs. the HFD group. (G) Kidney tissues immunohistochemically stained for α-SMA and collagen I. Scale bar, 20 μm; magnification, x400; n=3. $^*P<0.05$, $^{**}P<0.01$ vs. the control group; $^#P<0.05$ vs. the HFD group. α-SMA, α-smooth muscle actin; HFD, high-fat diet; Sal, salubrinal.

fibrosis, which may also be related to responses such as the inflammatory response, insulin resistance and oxidative stress.

The ER is the main location for the synthesis of secretory and transmembrane proteins, folding and maturation, Ca^{2+} storage and lipid biosynthesis (26). Various factors, such as genetic mutations, hypoxia, malnutrition and oxidative stress, can cause ERS. As a result of this response, the ER lumen is overloaded with unfolded and incorrectly folded proteins. Further activation

of the UPR contributes to a reduction in protein function and even cell death (27). Obesity is a chronic pathological stimulus associated with insulin resistance characterized by a state of low-grade inflammation (28), the main features of which include altered inflammatory signaling in adipocytes (29) and infiltration of immune cells into adipose tissue (30). Pathological expansion of adipose tissue leads to abnormal hypertrophy and thickening of adipocytes, resulting in adipocyte hypoxia, chronic low-grade
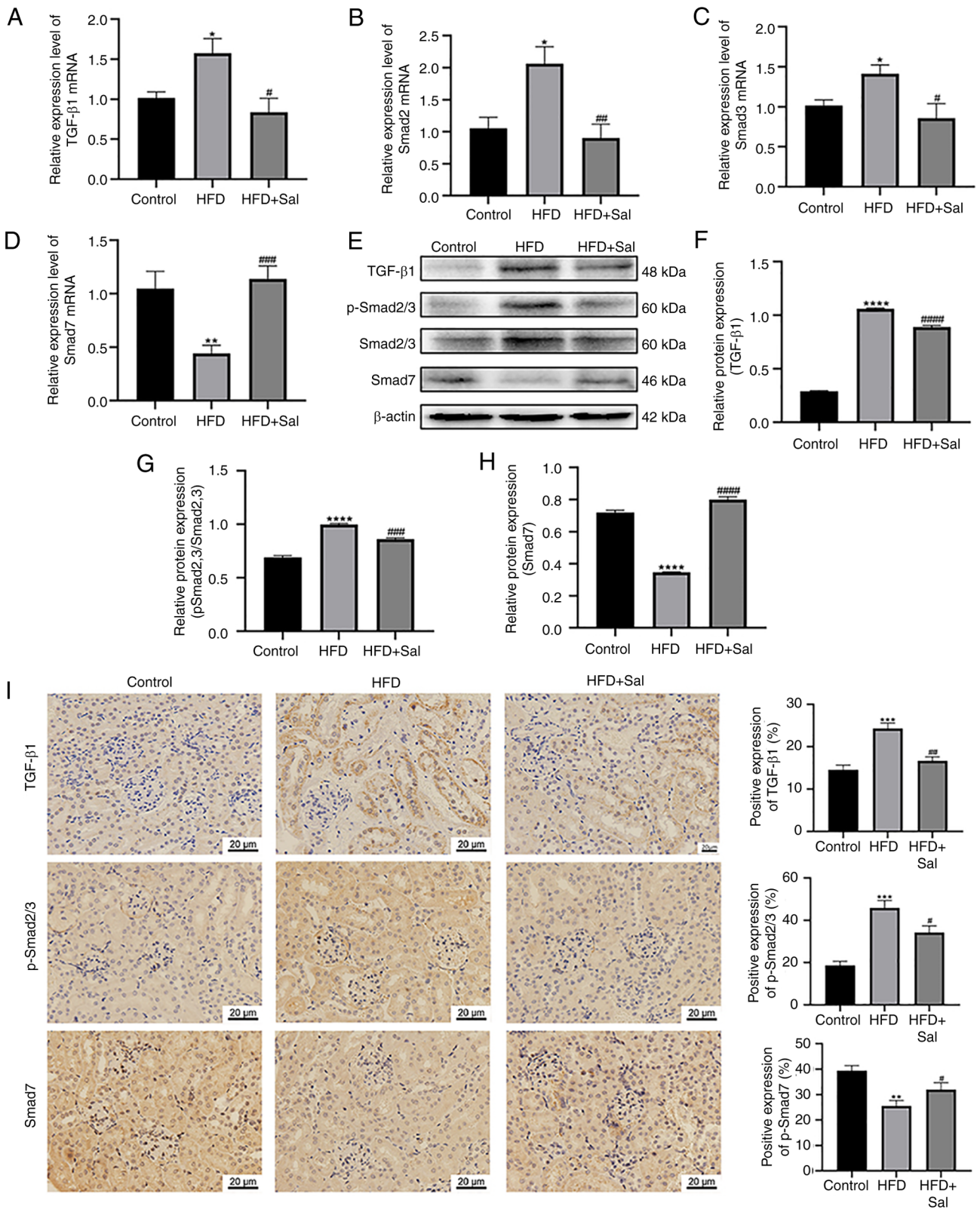
Figure 5. Activation of the TGF-β/SMAD pathway. The mRNA levels of (A) TGF-β1, (B) SMAD2, (C) SMAD3 and (D) SMAD7 in the kidney. (E-H) Western blotting was used to measure the levels of proteins, including those involved in the TGF-β/SMAD pathway. *P<0.05, **P<0.01, ****P<0.0001 vs. the control group; #P<0.05, ##P<0.01, ###P<0.001, ####P<0.0001 vs. the HFD group. (I) Kidney tissues were immunohistochemically stained for TGF-β1, p-SMAD2/3 and SMAD7. Scale bars are 20 µm; magnification, x400; n=3. **P<0.01, ***P<0.001 vs. the control group; #P<0.05, ##P<0.01 vs. the HFD group. HFD, high-fat diet; p-, phosphorylated; Sal, salubrinal.

inflammation, decreased vascularization, decreased reactive oxygen species production and ERS (31). Together with the aforementioned findings, it was hypothesized that adipose tissue

dysfunction may be a common mechanism for HFD-induced renal fibrosis and stimulation of ERS in mice. It has been shown that HFD-fed rats exhibit hypothalamic ERS and the

modulation of hypothalamic GRP78 activity is associated with white adipose tissue browning (32). Xie *et al* (33) report that HFD and STZ-induced diabetes can lead to nephropathy and that the mechanism of injury may involve ERS and CHOP. Although there is much evidence that ERS plays a role in HFD-induced inflammation and tissue damage, there is little evidence that ERS plays a role in HFD-induced renal fibrosis. Therefore, ERS activity in the HFD and control groups was evaluated. The results revealed that the expression of ERS markers, such as GRP78 and CHOP, was increased in the kidney tissues of the mice in the HFD group compared with those in the control group, suggesting that ERS may be involved in HFD-induced kidney injury. In addition, the kidneys of the mice in the HFD group presented significant oxidative stress injury, suggesting that HFD induced oxidative stress. This is consistent with previous finding that HFD can cause ERS and oxidative stress (31).

TGF-β1 is a versatile cytokine that regulates several cellular processes and extracellular matrix (ECM) components. It also plays an essential role in fibrogenesis and EMT. TGF-β1 specifically regulates the upstream EMT molecules SMAD2, SMAD3, SMAD4 and SMAD7, the last of which inhibits SMAD3 expression (34). Furthermore, TGF-β1 expression is upregulated during the fibrotic process in the lung, liver, kidney and other organs (34-36). Numerous investigations have demonstrated the strong relationships among ECM gene regulation, fibrogenesis and the TGF-β pathway (37). Inflammatory cytokines, such as elements of the TGF-β superfamily, different interleukins, oxidative damage and inflammation, are the major factors that govern fibrosis (38,39). Among these variables, TGF-β is a critical modulator of fibrogenesis. Renal fibrosis and kidney disorders are regulated by the TGF-β/SMAD pathway (38). The activity of the TGF-β1 receptor causes SMAD7 to separate from the receptor, activating and phosphorylating SMAD2 and SMAD3 (40,41). In the present study, mice in the HFD group presented increased expression of TGF-β1 and p-SMAD2/3 and decreased expression of SMAD7, suggesting that HFD may promote fibrosis in mice through activation of the TGF-β/SMAD pathway, a process that may be related to ERS.

For further validation, treatment with the ERS inhibitor Sal decreased the expression of TGF-β1 and p-SMAD2/3 and increased the expression of SMAD7. These findings suggested that Sal protects against renal fibrosis in HFD-fed mice through this pathway, which may be a possible route by which ERS induces renal fibrosis in HFD-fed mice. HFD triggers this pathway via ERS, which promotes the expression of TGF-β1 and SMAD2/3 while decreasing the expression of SMAD7. This leads to increased ECM deposition, which ultimately leads to renal fibrosis in mice (Fig. 6).

In conclusion, the present study revealed that renal fibrosis in HFD-fed mice is induced by ERS activation, which upregulates the TGF-β/SMAD pathway. These results provide important new insights into the mechanism of HFD-induced kidney injury and point to the possible therapeutic potential of inhibiting ERS regulation of renal fibrosis in the treatment of obese mice. The present study laid the groundwork for future directions, such as studies on important sites associated with HFD-induced obesity (brain and liver), as well as the extension of the experiments to *in vitro* to study the proliferation of fibroblasts and what causes them to proliferate and the factors that influence them.
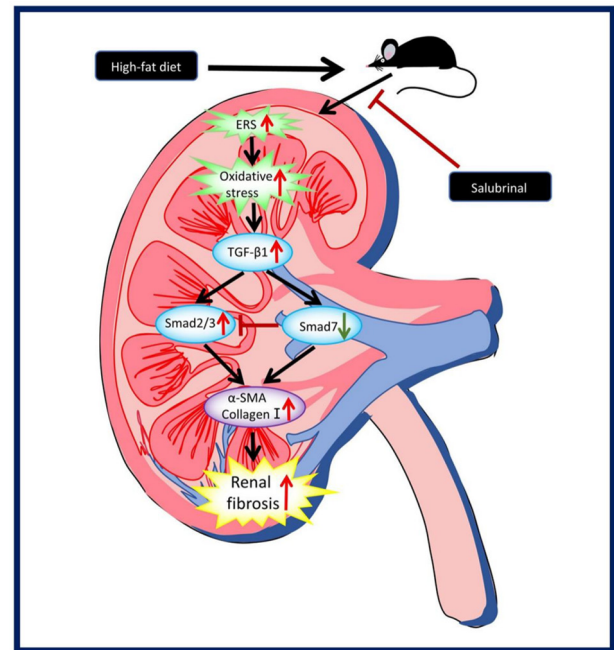

Figure 6. ERS induces renal fibrosis in high-fat diet mice via the TGF-β/SMAD pathway. HFD can induce ERS and oxidative stress in the kidneys of mice. ERS can activate the TGF-β/SMAD signaling pathway, leading to renal fibrosis in HFD-fed mice. However, the ER inhibitor Sal can protect the kidney by inhibiting this pathway. ERS, endoplasmic reticulum stress; HFD, high-fat diet; ER, endoplasmic reticulum; α-SMA, α-smooth muscle actin.

Acknowledgements

Funding

Availability of data and materials

The data generated in the present study may be requested from the corresponding author.

Authors' contributions

ZM and MC performed the research, established the obesity model, collected kidney specimens, analyzed the data and wrote the article. CL and BL designed and assisted with the experiments. JS and WG designed the experiments, provided overall guidance and helped with the manuscript. ZM and JS confirm the authenticity of all the raw data. All the authors read and approved the final manuscript.

Ethics approval and consent to participate

The experimental protocol of the present study was performed in accordance with the Guide for the Care and Use of

Laboratory Animals and approved by the Ethical Committee of Dali University (Yunnan, China; approval no. 2023-PZ-278).

Patient consent for publication

Not applicable.

Competing interests

The authors declare that they have no competing interests.

References

1. Jiang Z, Wang Y, Zhao X, Cui H, Han M, Ren X, Gang X and Wang G: Obesity and chronic kidney disease. Am J Physiol Endocrinol Metab 324: E24-E41, 2023.
2. Stasi A, Cosola C, Caggiano G, Cimmarusti MT, Palieri R, Acquaviva PM, Rana G and Gesualdo L: Obesity-related chronic kidney disease: Principal mechanisms and new approaches in nutritional management. Front Nutr 9: 925619, 2022.
3. Alizadeh S, Ahmadi M, Ghorbani Nejad B, Djazayeri A and Shab-Bidar S: Metabolic syndrome and its components are associated with increased chronic kidney disease risk: Evidence from a meta-analysis on 11 109 003 participants from 66 studies. Int J Clin Pract: May 23, 2018 (Epub ahead of print).
4. Huang R, Fu P and Ma L: Kidney fibrosis: From mechanisms to therapeutic medicines. Signal Transduct Target Ther 8: 129, 2023.
5. Liu S, Fu S, Jin Y, Geng R, Li Y, Zhang Y, Liu J and Guo W: Tartary buckwheat flavonoids alleviates high-fat diet induced kidney fibrosis in mice by inhibiting MAPK and TGF-β1/Smad signaling pathway. Chem Biol Interact 379: 110533, 2023.
6. Zhu X, Si F, Hao R, Zheng J and Zhang C: Nuciferine protects against obesity-induced nephrotoxicity through its hypolipidemic, anti-inflammatory, and antioxidant effects. J Agric Food Chem 71: 18769-18779, 2023.
7. Lee LE, Doke T, Mukhi D and Susztak K: The key role of altered tubule cell lipid metabolism in kidney disease development. Kidney Int 106: 24-34, 2024.
8. Zhang SX, Wang JJ, Starr CR, Lee EJ, Park KS, Zhylkibayev A, Medina A, Lin JH and Gorbatyuk M: The endoplasmic reticulum: Homeostasis and crosstalk in retinal health and disease. Prog Retin Eye Res 98: 101231, 2024.
9. Chen X and Cubillos-Ruiz JR: Endoplasmic reticulum stress signals in the tumour and its microenvironment. Nat Rev Cancer 21: 71-88, 2021.
10. Metcalf MG, Higuchi-Sanabria R, Garcia G, Tsui CK and Dillin A: Beyond the cell factory: Homeostatic regulation of and by the UPR^{ER}. Sci Adv 6: eabb9614, 2020.
11. Merighi A and Lossi L: Endoplasmic reticulum stress signaling and neuronal cell death. Int J Mol Sci 23: 15186, 2022.
12. Ma K, Zhang Y, Zhao J, Zhou L and Li M: Endoplasmic reticulum stress: Bridging inflammation and obesity-associated adipose tissue. Front Immunol 15: 1381227, 2024.
13. Carnuta MG, Deleanu M, Barbalata T, Toma L, Raileanu M, Sima AV and Stancu CS: Zingiber officinale extract administration diminishes steroyl-CoA desaturase gene expression and activity in hyperlipidemic hamster liver by reducing the oxidative and endoplasmic reticulum stress. Phytomedicine 48: 62-69, 2018.
14. Wu L, Guo T, Deng R, Liu L and Yu Y: Apigenin ameliorates insulin resistance and lipid accumulation by endoplasmic reticulum stress and SREBP-1c/SREBP-2 pathway in palmitate-induced HepG2 cells and high-fat diet-fed mice. J Pharmacol Exp Ther 377: 146-156, 2021.
15. Paik J, Fierce Y, Drivdahl R, Treuting PM, Seamons A, Brabb T and Maggio-Price L: Effects of murine norovirus infection on a mouse model of diet-induced obesity and insulin resistance. Comp Med 60: 189-195, 2010.
16. Tian RD, Chen YQ, He YH, Tang YJ, Chen GM, Yang FW, Li Y, Huang WG, Chen H, Liu X and Lin SD: Phosphorylation of eIF2α mitigates endoplasmic reticulum stress and hepatocyte necroptosis in acute liver injury. Ann Hepatol 19: 79-87, 2020.
17. Livak KJ and Schmittgen TD: Analysis of relative gene expression data using real-time quantitative PCR and the 2(-Delta Delta C(T)) method. Methods 25: 402-408, 2001.
18. Tang WB, Ling GH, Sun L and Liu FY: Smad anchor for receptor activation (SARA) in TGF-beta signaling. Front Biosci (Elite Ed) 2: 857-860, 2010.
19. Hojs R, Ekart R, Bevc S and Vodošek Hojs N: Chronic kidney disease and obesity. Nephron 147: 660-664, 2023.
20. Hsu CY, Mcculloch CE, Iribarren C, Darbinian J and Go AS: Body mass index and risk for end-stage renal disease. Ann Intern Med 144: 21-28, 2006.
21. Iseki K, Ikemiya Y, Kinjo K, Inoue T, Iseki C and Takishita S: Body mass index and the risk of development of end-stage renal disease in a screened cohort. Kidney Int 65: 1870-1876, 2004.
22. Zhou S, Wu Q, Lin X, Ling X, Miao J, Liu X, Hu C, Zhang Y, Jia N, Hou FF, *et al*: Cannabinoid receptor type 2 promotes kidney fibrosis through orchestrating β-catenin signaling. Kidney Int 99: 364-381, 2021.
23. Kume S, Uzu T, Araki S, Sugimoto T, Isshiki K, Chin-Kanasaki M, Sakaguchi M, Kubota N, Terauchi Y, Kadowaki T, *et al*: Role of altered renal lipid metabolism in the development of renal injury induced by a high-fat diet. J Am Soc Nephrol 18: 2715-2723, 2007.
24. Stone RC, Pastar I, Ojeh N, Chen V, Liu S, Garzon KI and Tomic-Canic M: Epithelial-mesenchymal transition in tissue repair and fibrosis. Cell Tissue Res 365: 495-506, 2016.
25. Deng B, Yang W, Wang D, Cheng L, Bu L, Rao J, Zhang J, Xie J and Zhang B: Peptide DR8 suppresses epithelial-to-mesenchymal transition via the TGF-β/MAPK signaling pathway in renal fibrosis. Life Sci 261: 118465, 2020.
26. Li YE, Sowers JR, Hetz C and Ren J: Cell death regulation by MAMs: From molecular mechanisms to therapeutic implications in cardiovascular diseases. Cell Death Dis 13: 504, 2022.
27. Sims SG, Cisney RN, Lipscomb MM and Meares GP: The role of endoplasmic reticulum stress in astrocytes. Glia 70: 5-19, 2022.
28. Engin A: The pathogenesis of obesity-associated adipose tissue inflammation. Adv Exp Med Biol 960: 221-245, 2017.
29. Lumeng CN and Saltiel AR: Inflammatory links between obesity and metabolic disease. J Clin Invest 121: 2111-2117, 2011.
30. Olefsky JM and Glass CK: Macrophages, inflammation, and insulin resistance. Annu Rev Physiol 72: 219-246, 2010.
31. Sun K, Kusminski CM and Scherer PE: Adipose tissue remodeling and obesity. J Clin Invest 121: 2094-2101, 2011.
32. Contreras C, González-García I, Seoane-Collazo P, Martínez-Sánchez N, Liñares-Pose L, Rial-Pensado E, Fernø J, Tena-Sempere M, Casals N, Diéguez C, *et al*: Reduction of hypothalamic endoplasmic reticulum stress activates browning of white fat and ameliorates obesity. Diabetes 66: 87-99, 2017.
33. Xie H, Huang L, Li Y, Zhang H and Liu H: Endoplasmic reticulum stress and renal lesion in mice with combination of high-fat diet and streptozotocin-induced diabetes. Acta Cir Bras 31: 150-155, 2016.
34. Wang L, Wang HL, Liu TT and Lan HY: TGF-beta as a master regulator of diabetic nephropathy. Int J Mol Sci 22: 7881, 2021.
35. Ye Z and Hu Y: TGF-β1: Gentlemanly orchestrator in idiopathic pulmonary fibrosis (review). Int J Mol Med 48: 132, 2021.
36. Ahmed H, Umar MI, Imran S, Javaid F, Syed SK, Riaz R and Hassan W: TGF-β1 signaling can worsen NAFLD with liver fibrosis backdrop. Exp Mol Pathol 124: 104733, 2022.
37. Peng D, Fu M, Wang M, Wei Y and Wei X: Targeting TGF-β signal transduction for fibrosis and cancer therapy. Mol Cancer 21: 104, 2022.
38. Gifford CC, Tang J, Costello A, Khakoo NS, Nguyen TQ, Goldschmeding R, Higgins PJ and Samarakoon R: Negative regulators of TGF-β1 signaling in renal fibrosis; pathological mechanisms and novel therapeutic opportunities. Clin Sci (Lond) 135: 275-303, 2021.
39. Antar SA, Ashour NA, Marawan ME and Al-Karmalawy AA: Fibrosis: Types, effects, markers, mechanisms for disease progression, and its relation with oxidative stress, immunity, and inflammation. Int J Mol Sci 24: 4004, 2023.
40. de Ceuninck van Capelle C, Spit M and Ten Dijke P: Current perspectives on inhibitory SMAD7 in health and disease. Crit Rev Biochem Mol Biol 55: 691-715, 2020.
41. Gu YY, Liu XS, Huang XR, Yu XQ and Lan HY: Diverse role of TGF-β in kidney disease. Front Cell Dev Biol 8: 123, 2020.